第 27 卷第 3 期 无 机 化 学 学 报 Vol.27 No.3
2011 年 3 月 CHINESE JOURNAL OF INORGANIC CHEMISTRY 547-555

Bi_2O_3/TiO_2 复合纳米颗粒的可见光光催化性能

杨 娟* 李建通 缪 娟
(河南理工大学理化学院,焦作 454003)

摘要: 采用溶胶与水热相结合的方法合成了具有可见光光催化活性的复合纳米颗粒 Bi_2O_3/TiO_2, 并对其进行了 X 射线衍射、透射电镜、X 射线光电子能谱、紫外-可见漫反射谱、红外光谱、低温 N_2 吸附脱附及电子顺磁共振分析。结果表明,复合少量的氧化铋可显著抑制 TiO_2 由锐钛矿到金红石的相转移过程,并将光吸收范围扩展到可见光区。可见光照射下(λ>420 nm),利用电子顺磁共振技术检测到明显的羟基自由基(·OH)信号。铋的最佳掺杂量为 Bi/Ti 质量比 2.0%,适量铋的掺入能显著改善锐钛矿 TiO_2 的结晶度,抑制光生电子-空穴对的复合,提高光催化量子效率。通过可见光照射下,4-氯酚的降解实验测试 Bi_2O_3/TiO_2 复合纳米颗粒的可见光光催化活性。同时,利用气-质联用仪对 4-氯酚降解过程的中间产物进行了测定,并提出可见光照射下的 Bi_2O_3 光敏化机理。

关键词: 氧化铋; TiO_2; 可见光; 光催化; 4-氯酚
中图分类号: O643.3; O614.41 **文献标识码**: A **文章编号**: 1001-4861(2011)03-0547-09

Visible Light Photocatalytic Performance of Bi_2O_3/TiO_2 Nanocomposite Particles

YANG Juan* LI Jian-Tong MIAO Juan
(*Department of Physics and Chemistry, Henan Polytechnic University, Jiaozuo, Henan* 454003, *China*)

Abstract: Visible-light photoactive Bi_2O_3/TiO_2 catalysts were prepared by sol-hydrothermal process. The as-prepared samples were characterized by XRD, TEM, XPS, UV-Vis diffuse reflectance spectroscopy (UV-Vis DRS), FTIR, N_2 adsorption-desorption and ESR. Compounding with low amounts of Bi_2O_3 could effectively inhibit the phase transformation from anatase to rutile. UV-Vis DRS showed an extension of light absorption into the visible region. ESR results indicated that the active species (·OH) was generated with visible illumination (λ>420 nm). It was found that the optimal dosage of bismuth was 2.0wt%. Proper amount of bismuth species compounded on the TiO_2 surface could improve the anatase crystallinity, which could inhibit the recombination between photoelectrons and holes, leading to enhanced photocatalytic quantum efficiency. Meanwhile, the enhanced visible-light activity was tested by the photocatalytic degradation of 4-chlorophenol (4-CP). Furthermore, the generated intermediates were identified using gas chromatograph-mass spectrometer and Bi_2O_3-photosensitization mechanism under visible light illumination was proposed.

Key words: bismuth oxide; TiO_2; visible light; photocatalysis; 4-chlorophenol

Powdered titania have been proven to be excellent photocatalytic materials for degradation of organic pollutants under UV irradiation[1-2]. However, the wide band gap of TiO_2 (anatase of 3.2 eV, rutile of 3.0 eV) limits the absorption wavelength to less than 387 nm, which is only 3%~5% of the sunlight energy. Therefore, the development of visible-light photocatalysts is indispensable to be able to utilize the major portion of

收稿日期:2010-10-08。收修改稿日期:2010-11-25。
国家自然科学基金(No.51074067),河南省教育厅自然科学基金(No.2010B150009)资助项目。
*通讯联系人。E-mail:yangjuan0302@yahoo.cn

the solar spectrum and to realize indoor application of photocatalysts.

Thus far, a lot of efforts have been devoted to modify the photocatalyst[3-5]. Among the studies, an important strategy to extent the light absorption property of TiO_2 is the formation of heterojunction between TiO_2 and a sensitizer semiconductor with a narrow bandgap[6-8]. In the heterojunction structure, the sensitizer is excited by visible light irradiation, and some of the photogenerated electrons and holes will then be transferred to TiO_2. Bi_2O_3, with a direct band gap 2.8 eV, thus will be able to absorb some portion of visible light (λ <440 nm) and decompose the organic pollutants[9-10]. But alone, its photocatalytic activity is very low, owing to the high electron-hole recombination rate in Bi_2O_3[11]. On the other hand, Bi_2O_3 can act as an effective photosensitizer and form the coupled semiconductor with TiO_2. Rengaraj and Li[12] reported that Bi^{3+}-TiO_2 could improve the photocatalytic reduction of nitrate in aqueous solution under UV illumination. Jing et al.[13] demonstrated that Bi_2O_3-compounded TiO_2 could improve the photocatalytic decomposition of dyes pollutant rhodamine B (RhB). Bian et al.[14] synthesized active Bi_2O_3/TiO_2 visible photocatalyst with ordered mesoporous structure and highly crystallized anatase by evaporation-induced self-assembly method. However, to the best of our knowledge, there has been no reports of systematic studies on effects of the bismuth content on the TiO_2 phase transformation and the photoinduced charge properties by ESR technique, together with their relationships with the enhanced photocatalytic activity and degradation approach of 4-CP under visible-light irradiation.

In the present work, we prepared Bi_2O_3/TiO_2 photocatalysts by sol-hydrothermal method with different contents of bismuth. The prepared materials were characterized by XRD, TEM, XPS, UV-Vis DRS, FTIR and ESR spectroscopy. The enhanced photocatalytic activity was tested in the degradation of 4-CP under visible illumination, which was chosen as probe molecule, due to its environmental importance as priority toxic pollutant[15]. The promoting mechanism on the activity from the high anatase crystallinity, the optical response extent, the increasing surface OH group density and the effective photosensitizating effect of Bi_2O_3 were examined. Meanwhile, by the examination of the intermediates with GC-MS, the photocatalytic mechanism and the possible approach of visible-light degradation for 4-CP were also discussed.

1 Experimental

1.1 Reagents and materials

Titanium tetra-*n*-butoxide ($Ti(O\text{-}Bu)_4$) and bismuth nitrate with analytical grade were obtained from Aldrich Chemical Co. Glycolic acid, succinic acid, fumaric acid, malic acid, 1,1,1,3,3,3-hexamethyldisilazane, Chlorotrimethylsilane and anhydrous pyridine were purchased from J&K chemical Ltd. 4-CP, hydroquinone and all other chemicals were of analytical grade used without further purification.

1.2 Photocatalysts preparation

The Bi_2O_3/TiO_2 samples with different percentages of bismuth (0.5%, 1%, 2%, 4% and 5%, (*w*/*w*)) were prepared by sol-hydrothermal method, using $Bi(NO_3)_3$ and $Ti(O\text{-}Bu)_4$ as precursors. In a typical process, 10 mL of $Ti(O\text{-}Bu)_4$ was dissolved in 10 mL of ethanol by stirring vigorously to produce $Ti(O\text{-}Bu)_4$-C_2H_5OH solution. Meanwhile, 10 mL of water, 2 mL of 16 mol·L^{-1} HNO_3 and the desired amount of $Bi(NO_3)_3$ were added to another 40 mL of C_2H_5OH to form an ethanol-nitric acid-water solution. Consequently, the $Ti(O\text{-}Bu)_4$-C_2H_5OH solution was slowly added dropwise to the latter solution under vigorous stirring to carry out a hydrolysis. The obtained semitransparent sol was transferred to a 100 mL Teflon autoclave and kept at 140 ℃ under authigenic pressure for 6 h for hydrothermal treatment. Then, the autoclave was cooled to room temperature and the precipitates obtained were separated by centrifugation, washed thoroughly with deionized water and ethanol, dried at 90 ℃ overnight, and calcined in air at 500 ℃ for 2 h. A TiO_2 sample was also prepared by the same procedure except without the addition of the bismuth precursor.

1.3 Photocatalyst characterization

The crystallographic properties were investigated by a Philips X′Pert PRO X-ray diffractometer using

Cu *Kα* radiation (λ=0.154 18 nm), in which an accelerating voltage of 40 kV and an emission current of 30 mA over the 2θ range of 10°~90°. The settings for XRD examination were as follows: divergence slit, 1 mm; graphite monochromator; anti-scatter slit, 2 mm; receiving slit, 0.15 mm; scintillator detector. The particle size was estimated using the Scherrer equation. The morphologies were observed by a transmission electron microscopy (TEM, JEOL JEM-2010). N_2 adsorption-desorption isotherms were collected at 77 K by using Micromeritics ASAP 2020 Surface Area & Pore Size Analyzer. IR spectrum was recorded as KBr pellets on Bruker Fourier transform infrared (FTIR) spectrometer. The ultraviolet-visible diffuse reflectance spectra (UV-Vis DRS) of the samples in the wavelength range 250~750 nm were recorded using a spectrophotometer (Hitachi U-3010), with $BaSO_4$ as a reference. Surface electronic states were analyzed by X-ray photoelectron spectroscopy (XPS, Axis Ultra, Kratos analytical Ltd.) with Al *Kα* X-ray source. All binding energies were calibrated by using the contaminant carbon (C1*s* 284.6 eV) as a reference. The electron spin resonance (ESR) signals of radicals trapped by 3,4-Dihydro-2,2-dimethyl-2*H*-pyrrole 1-oxide (DMPO, CAS No: [3317-61-1]) were detected at ambient temperature on a Bruker (E 500) spectrometer. The irradiation source was the same as used in the degradation of 4-CP. The settings for the ESR spectrometer were as follows: center field, 3480 G; sweep width, 100 G; microwave frequency, 9.64 GHz; modulation frequency, 100 kHz; power, 10.05 mW.

1.4 Photocatalytic reaction

The photocatalytic degradation of 4-CP was carried out at 25 ℃ in an 75 mL self-designed glass photochemical reactor containing 0.050 g of catalyst and 50 mL of 1.0×10^{-4} mol·L^{-1} 4-CP aqueous solution. Prior to photoreaction, the suspension was magnetically stirred in dark for 30 min to establish an adsorption/desorption equilibrium. The suspension was vertically irradiated from the top by a 300 W Xenon lamp (Changtuo Instrumental Corporation of Beijing) at constant stirring speed. All the UV lights with wavelength shorter than 420 nm were removed by a glass filter (JB-420). At the given time intervals, the analytical samples were taken from the suspension and immediately centrifuged at 4 000 r·min^{-1} for 10 min, then filtrate through a 0.22 μm Millipore filter to remove particles. The filtrate was analyzed by HPLC for the degree of 4-CP degradation.

The concentrations of 4-CP were measured by HPLC using an Agilent 1200 HPLC with a diode-array detector (G1315C) and a 1200 series binary pump. An Intersil ODS-3C-18, 5 μm 4.6×250 mm column was used. Substances were routinely quantified from their absorbance at 280 nm. The eluent was 60% aqueous methanol and 40% phosphate buffer solution (0.1%, *V*/*V*). GC-MS data were obtained on an Agilent 6890 gas chromatograph using a 25 m 0.20 mm×0.33 μm DB-5 column, coupled with an Aglient 5985 mass spectrometer. The temperature program was as follows: at 50 ℃, hold time=6.5 min; from 50 to 200 ℃, rate=10 ℃·min^{-1}. The injector port was set for split operation at 250 ℃. The samples after irradiation were filtered, and the filtrate was then concentrated by a rotary evaporator and freeze-dried overnight. The residue was finally redissolved in 0.1 mL anhydrous pyridine, followed by the addition of 0.1 mL hexamethyldisilazane and 0.05 mL of chlorotrimethylsilane[16]. The silylated sample was further analyzed by GC-MS.

Total organic carbon was measured by a Tekmar Dohrmann Apollo 9000 TOC analyzer. The concentration of the chloride ions produced was determined using a chloride ion selective electrode. The K_2HPO_4 was used for the buffer solution and to adjust the ionic strength.

2 Results and discussion

2.1 XRD, TEM and XPS characterization

XRD peaks at 2θ=25.28° and 2θ=27.40° are often taken as the characteristic peaks of anatase (101) and rutile (110) crystal phase, respectively. Fig.1 shows the XRD patterns of pure TiO_2 and modified samples with different bismuth contents. The percentage of anatase in the samples can be estimated from the respective integrated XRD peak intensities using the quality factor ratio of anatase to rutile (1.265), and the crystal sizes

can also be calculated using the Scherrer equation[17].

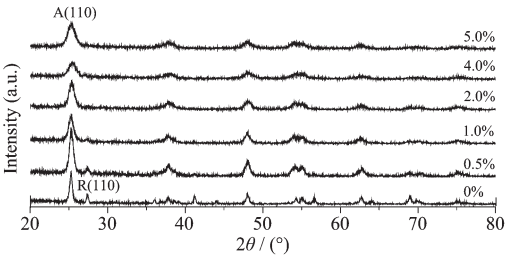

Fig.1 XRD patterns of the pure TiO_2 and Bi-modified TiO_2 calcined at 773 K

From Fig.1, it can be seen that pure TiO_2 have significant diffraction peaks representing the characteristic of anatase phase around 2θ of 25.2°, 37.9°, 47.8°, 53.8°, 55.0°, 62.1°, 62.7°, 68.8°, 70.3° and 75.1°, respectively. However, about 19.6% of rutile was also detected, implying that there is some phase transformation in the present experimental conditions. Compared with pure TiO_2, the modified TiO_2 with 0.5% or 1.0% bismuth exhibits lower rutile characteristic peak. These two samples contained about 12.4% and 5.5% rutile phase. When the bismuth content increases to 2.0%, or more than 2.0%, no rutile phase is detected in the bismuth-compounded TiO_2 samples. These results demonstrate that the surface-modification with Bi can inhibit effectively the phase transformation from anatase to rutile, which is favorable to the improvement of the anatase crystallinity. The high crystallization degree of anatase facilitates the rapid transfer of photoelectrons from bulk to the surface, which could effectively inhibit the recombination between photoelectrons and holes, leading to enhanced photocatalytic quantum efficiency[18]. However, the crystallization degree and sizes of Bi_2O_3 /TiO_2 decrease slightly with the increase of bismuth contents, as mainly evidenced by the intensity and the full width at the half maximum (FWHM) value of their characteristic XRD peaks. The reason may be that the presence of bismuth disturbs the crystallization process during calcination[19].

TEM images of TiO_2 nanoparticles uncompounded (A) and compounded with 2.0% Bi (B) are shown in Fig. 2. The dispersion of TiO_2 nanoparticles is markedly improved by compounding Bi. It can be also seen that the both samples display similar spherical form, with the particle size of 20~25 nm and 10~15 nm, respectively, demonstrating that compounding Bi can inhibit the growth of TiO_2 nanoparticles. Additionally, individual particles sizes in Fig.2 are comparable with those obtained by the Scherrer equation (Table 1), which demonstrates the particles are mainly mono-disperse and non-agglomerate.

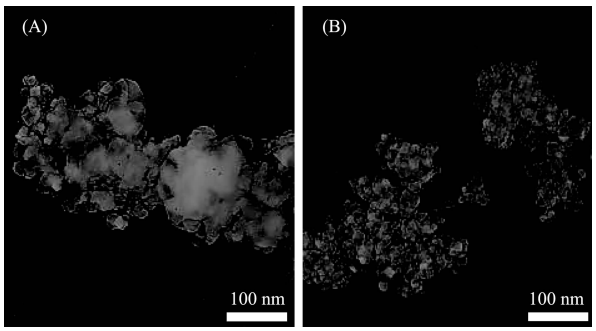

Fig.2 TEM images of TiO_2(A) and 2.0% Bi-compounded TiO_2 (B) powder

The XPS spectrum of 2.0% Bi-modified TiO_2 and the high-resolution XPS spectrum of Bi4*f* are shown in Fig.3. The peaks centered at 158.6 and 163.9 eV could be assigned to Bi4$f_{7/2}$ and Bi4$f_{5/2}$ region[20]. The presence of Bi_2O_3 exerts no significant influence on the XPS spectra in either the Ti2*p* or O1*s* orbitals. Moreover, the XRD peaks of Bi-compounded TiO_2 do not shift much compared with bare TiO_2. These results demonstrate

Table 1 Crystallite size, anatase phase composition and apparent rate constants of the as prepared TiO_2 samples

Sample	Pure TiO_2	0.5%	1.0%	2.0%	4.0%	5.0%
Crystallite size, *D* / nm						
Anatase (101)	22	17	14	12	10	9
Rutile (110)	23	18	15	—	—	—
Anatase phase composition / %	80.4	87.6	94.5	100	100	100
Apparent rate constant, K_{app} / min^{-1}	0.000 1	0.009	0.001 7	0.003 1	0.002 8	0.002 6
Regression relative coefficient, R^2	0.984	0.990	0.986	0.992	0.984	0.986

Note: 0.5%, 1.0%, 2.0%, 4.0% and 5.0% represent the weight percentage of Bi-compounded TiO_2, respectively.

that the Bi_2O_3 is present mainly as a separate phase, which is ascribed to the larger size of Bi atom (103 pm) than that of Ti atom (61 pm)[12].

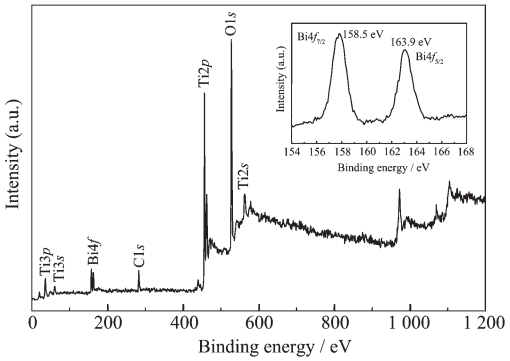

Inset: the high-resolution XPS spectrum of Bi4*f*

Fig.3　XPS spectrum of 2.0% Bi-compounded TiO_2

2.2　Optical absorption properties of photocatalysts

The surface hydroxyl groups on titania have been recognized to play an important role on the photocatalytic reaction. Fig.4 shows the FTIR spectra of different TiO_2 samples diluted and pressed in KBr dics. The strong and broad IR band of curve a and b between 400~850 cm^{-1} correspond to the Ti-O stretching vibration modes in crystal TiO_2[21]. With the increase in bismuth content, the additional peak around 489 cm^{-1} appears due to the vibrations from Bi-O bonds[22], as displayed in curve c, d, e and f. The IR peak at 1 630 cm^{-1} is ascribed to the bending vibration of O-H bonds of adsorbed water strongly bound to the catalyst surface[23-24]. The broad absorption peaks near 3 400 cm^{-1} are attributed to the stretching mode of O-H bond, which is related to water molecules and crystal surface hydrogen bonding. Obviously, as the bismuth content of modified TiO_2 samples increases, the amount of surface hydroxyl gradually increases. The larger surface hydroxyl group density will lead to the enhancement of the photocatalytic activity. Because the larger surface hydroxyl group can interact with photogenerated holes, giving better charge transfer and inhibiting the recombination of electron-hole pairs.

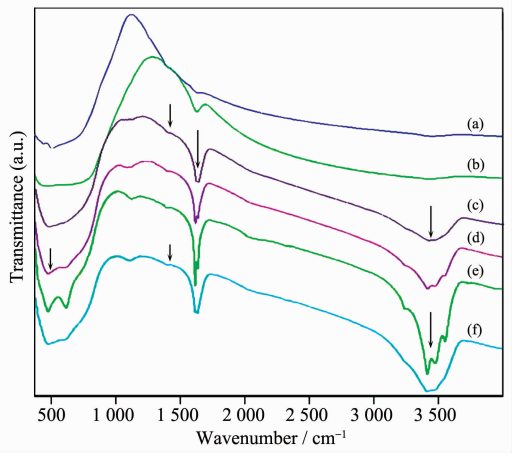

(a) Pure TiO_2, (b) 0.5% Bi-TiO_2, (c) 1.0% Bi-TiO_2, (d) 2.0% Bi-TiO_2, (e) 4.0% Bi-TiO_2, (f) 5.0% Bi-TiO_2, respectively

Fig.4　FTIR spectra of the prepared photocatalysts

As shown in Fig.5, the UV-Vis DRS spectra demonstrate that the pure TiO_2 displays no significant absorbance in the visible region due to the big energy gap (3.2 eV). With the introduction of Bi ions, the absorption edge shifts towards longer wavelengths (400~600 nm). The absorbance of Bi_2O_3/TiO_2 has similar intensity with the Bi content from 0.5%~2.0%. Meanwhile, further increase of the Bi content is bene-ficial to the light absorbance. The absorbance of Bi_2O_3 /TiO_2 increases with Bi content, suggesting that the spectral response in the visible region mainly results from Bi_2O_3 photosensitization[9]. Briefly, the Bi_2O_3 photo sensitizer with narrow energy gap (2.8 eV) could be easily activated by visible lights and induce photoelec-trons and holes. The photo-holes in bismuth oxide could easily transfer from the valence band (VB) of Bi_2O_3 to the neighboring VB of TiO_2[25]. Thus, the Bi_2O_3-TiO_2 heterojunctions formed in the composite TiO_2 could effectively inhibit the recombination between photoelectrons and holes, leading to the strong response in visible area.

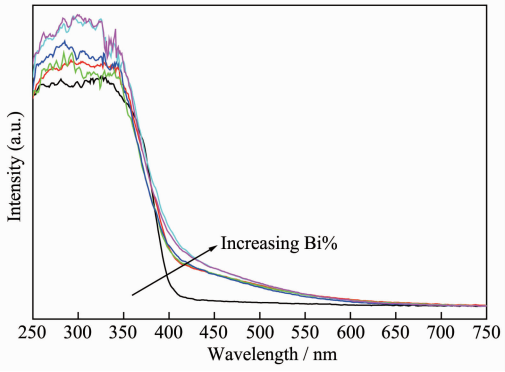

Fig.5　UV-Vis DRS spectra of the pure TiO_2 and Bi-modified TiO_2 calcined at 773 K

2.3 ESR signal analysis of DMPO-·OH

Spin-trapping ESR technique was employed to identify the possible short-lived reactive oxygen species involved in the photocatalytic systems. For this study, all the ESR spectra were recorded by the same irradiation as used in the photocatalytic degradation using DMPO as the radical trapping agent, and the ESR signals at different irradiation time are shown in Fig.6.

It can be seen from Fig. 6, no ESR signals are observed when the photocatalysis is performed in the dark in the presence of catalyst and DMPO. Under visible light illumination, it is evident that in the pure TiO_2 system, no signal (1:2:2:1 signals) of the DMPO-·OH radical adducts is observed during the degradation process (Fig.6A). Whereas, the generation of ·OH species is confirmed by ESR technique when irradiated with visible light for the 2.0% Bi-TiO_2 system (Fig. 6B)[26]. The results may reveal why 2.0% Bi-TiO_2 exhibits much higher activity than bare TiO_2. Moreover, the intensity of the peaks further increases with the increase of irradiation time and reaches stable state in 15 min, therefore the intensity of DMPO-·OH adduct peak produced in 20 min irradiation is similar to that in 15 min irradiation.

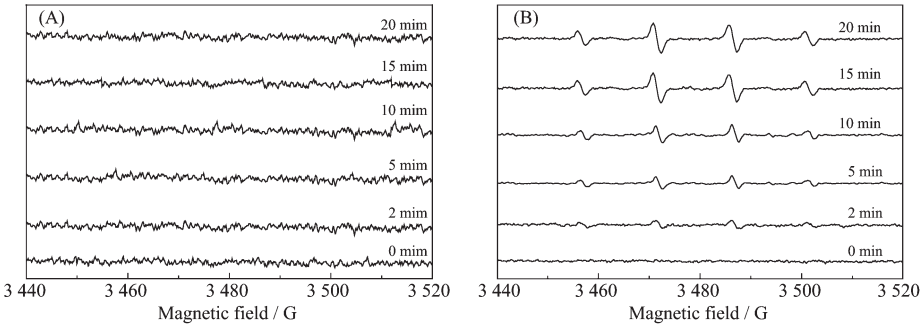

Fig.6 DMPO spin-trapping ESR spectra of (A) pure TiO_2 and (B) 2.0% Bi modified-TiO_2 aqueous solutions

2.4 Photocatalytic degradation of 4-chlorophenol

In order to evaluate the photocatalytic activity of the prepared catalysts and find out the optimum content of Bi species, a set of experiments for 4-CP degradation under visible-light irradiation was carried out in and the results are shown in Fig.7A. The pure TiO_2 is rather inefficient since it could not be activated by visible lights due to a big energy band gap (3.2 eV). Modification of TiO_2 with Bi_2O_3 results in abrupt increase of the photocatalytic activity owing to the Bi_2O_3-photosensitization. It is found that pseudo-first-order kinetics is obeyed for the photocatalytic degradation of 4-CP. Therefore, the apparent first order kinetic Eq.(**1**) is used to fit the experimental data in Fig. 7A.

$$\ln\frac{C_0}{C}=k_{app}t \qquad (\mathbf{1})$$

Where k_{app} is the apparent rate constant, C is the concentration of 4-CP remaining in the solution at irradiation time of t, and C_0 is the initial concentration

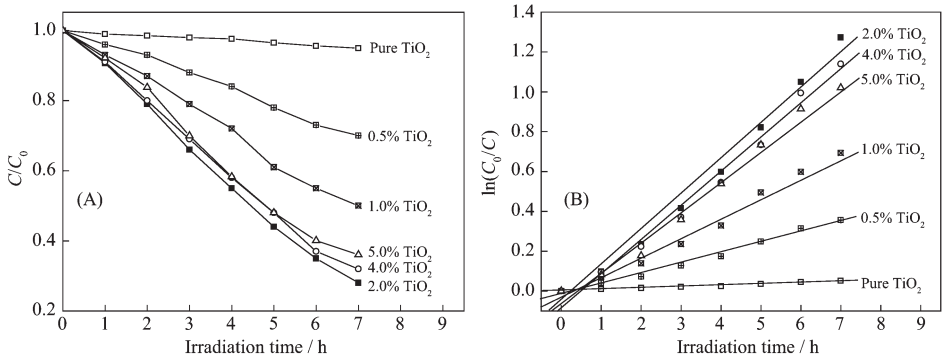

Fig.7 (A) Photocatalytic kinetics of 4-CP degradation for pure TiO_2 and Bi-modified TiO_2; (B) Variations in $\ln(C_0/C)$ as a function of irradiation time and linear fits of pure TiO_2 and Bi-compounded TiO_2

at t=0. The variation in $\ln(C_0/C)$ as a function of irradiation time are given in Fig.7B. The calculated data are given in Table 1.

The results of Fig.7B and Table 1 show that the effectiveness of the catalyst is strongly dependent on the amount of dopant ions. The 4-CP degradation efficiency after 7 h follows the order: 2.0% Bi-TiO_2 > 4.0%Bi-TiO_2 > 5.0%Bi-TiO_2 > 1.0%Bi-TiO_2 > 0.5%Bi-TiO_2. The experimental results are also related to BET specific surface area of Bi-modified TiO_2. For instance, the BET specific surface area of 2.0% Bi-TiO_2 is 130 $m^2 \cdot g^{-1}$, which is much higher than 33 $m^2 \cdot g^{-1}$ of bare TiO_2. The larger specific surface area provides larger contact area and will lead to higher photo-degradation efficiency. Among the Bi-compounded TiO_2, 2.0% (wt) Bi-TiO_2 catalyst exhibits the highest activity under visible illumination. However, very high Bi content (> 2.0%) is harmful for the photocatalytic activity because of the agglomeration of the Bi_2O_3 particles. The high Bi contents facilitates charge transport and reduces charge recombination, the large nanoparticles may act as the centers of electron-hole recombination and reduce quantum efficiency[27].

2.5　Mineralization and dechlorination

From an application perspective, analysis of degradation products is useful to estimate the efficiency of the photocatalytic technique, and it also may help reveal details of the chemical process taking place during the degradation and mineralization. To identify the intermediates of 4-CP degradation, GC-MS analysis was used. The unfunctionalized degradation mixture is not suitable for GC-MS analysis, so the mixtures were silylated with TMS groups. The GC-MS results demonstrate the hydroxylated intermediates, such as catechol, hydroquinone, 4-chlorocatechol and 4-chlororesorcinol, were firstly generated during the photodegradation of 4-CP. The primary products mainly involves the addition of HO· to aromatic ring and substitution of chlorine by HO·. Subsequently, under the effect of HO· radicals, the hydroxylated intermediates were further oxidated and resulted in the formation of a series of low molecular weight carboxylic acids through the cleavage of benzene rings, which were also analyzed by GC-MS. The aliphatic intermediates are mainly dicarboxylic acids and substitutional dicarboxylic acids, such as oxalic acid, glycolic acid, malonic acid, maleic acid, succinic acid, fumaric acid, tartronic acid, malic acid and tartaric acid. In most instances, these structural assignments were confirmed with samples of authentic material that was processed in the same way that showing the same chromatographic and MS behavior. However, other reasonable pathways also maybe exist to get to these compounds.

Meanwhile, during the photocatalytic degradation of 4-CP, the attack of HO· to 4-CP may replace chlorine atoms and produced organic dicarboxylic acids before complete mineralization. To examine the extent of mineralization of 4-CP under visible light illumination, both removal yield of TOC and the quantity of inorganic chloride ions released were determined.

Temporal changes of TOC and variations in the concentration of Cl^- are shown in Fig.8. The initial 4-CP contains 13.9 $mg \cdot L^{-1}$ of TOC. After the adsorption of 4-CP on the 2.0% Bi-TiO_2 surface, the TOC values in the supernatants drop to 12.6 $mg \cdot L^{-1}$. The rate of TOC reduction is remarkably slower than that of 4-CP. About 62% of TOC still remains after 13 h irradiation when the release of Cl^- occurrs to a greater extent during the degradation of 4-CP. The maximum extent of dechlorination is ca. 76% (1.52×10^{-4} $mol \cdot L^{-1}$), which is close to the theoretical quantity of about 1.60×10^{-4} $mol \cdot L^{-1}$ (the quantity of 4-CP degradation). It can be concluded from this result that dechlorination of 4-CP is completed but about half of 4-CP is mineralized into

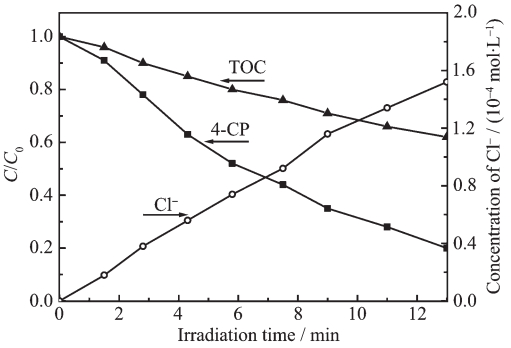

Fig.8　Change in 4-CP concentration and TOC and the formation of Cl^- during the degradation of 4-CP (2×10^{-4} $mol \cdot L^{-1}$) in the presence of 2.0% Bi-TiO_2

CO_2 and H_2O.

2.6 Cyclic experiments

Based on the above results, one could conclude that 2.0% Bi modified-TiO_2 exhibit the highest activity under visible irradiation. Besides the high activity, the 2.0% Bi-TiO_2 also displays strong durability. As shown in Fig.9, only 3% decrease in activity is observed even after being used repetitively for 8 times, which demonstrates that this catalyst is quite stable during liquid-phase photocatalytic degradation.

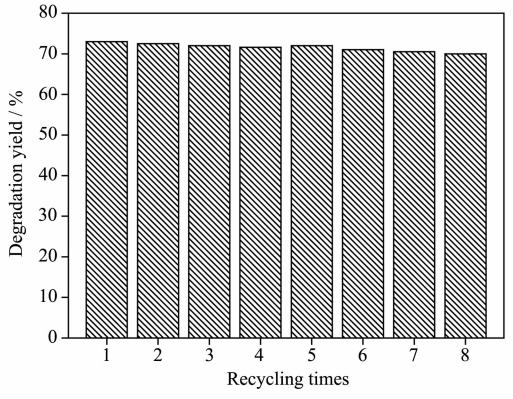

Reaction condition: 50.0 mL solution of 1.0×10^{-4} mol·L^{-1} 4-CP, 1 g·L^{-1} catalyst, visible light illumination

Fig.9 Recycling tests of the 2.0% Bi-TiO_2 photocatalyst

2.7 Proposed mechanism and possible degradation pathway

In the absence of Bi_2O_3, the titania cannot be directly excited by visible light. Modification of TiO_2 with Bi_2O_3 could prevent phase transition from anatase to rutile and lead to the strong spectral response in visible region, as indicated in Fig.1 and Fig.5. The abrupt increase of the photocatalytic activity of 4-CP degradation ascribes the Bi_2O_3-photosensitization. Briefly, the Bi_2O_3 photosensitizer with narrow energy gap (2.8 eV) could be easily activated by visible light and induce photoelectrons and holes. In the absence of TiO_2, these electrons and holes might recombine rapidly, leading to the quenching of spectral response.

In Bi_2O_3/TiO_2 system, the heterojunctions formed in the composite catalyst would promote the photo-generated holes in bismuth oxide to be transferred to the upper lying valence bands of titania, because the valence band of Bi_2O_3 is lower than that of titania (as shown in Fig.10). The process is thermodynamically feasible[28]. Therefore, the recombination between photo-electrons and holes could be effectively inhibited and much more holes are captured to generate hydroxyl radicals and/or further induce photocatalytic reactions. Accordingly, the distinct difference of ESR signals observed between the 2.0% Bi-modified TiO_2 and pure TiO_2 dispersions is understandable. As a result, the photocatalytic activity of Bi_2O_3/TiO_2 composite photocatalyst enhances a lot compared to the pure TiO_2. Based on the identification of intermediate products, the degradative process of 4-CP firstly undergoes the hydroxylation or dechlorination reaction induced by active hydroxyl radicals. After that, these hydroxylated intermediates are oxidated and a series of dicarboxylic acids or substitutional dicarboxylic acids are generated.

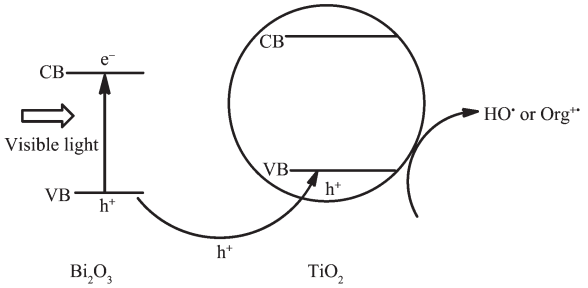

Fig.10 Bi_2O_3-photosensitizating mechanism of 2.0% Bi-TiO_2 under visible light irradiation

3 Conclusions

Bi_2O_3/TiO_2 composite photocatalyst was synthesized by the sol-hydrothermal method and characterized by XRD, TEM, XPS, FTIR, UV-Vis DRS and ESR techniques. The promoted activity of such Bi_2O_3/TiO_2 mainly derives from the high anatase crystallinity, the optical response extent and the strong photosensitizing effect of Bi_2O_3. The enhanced photocatalytic activity of the material was evaluated on the visible light photodegradation of 4-CP. TOC analysis shows that the mineralization of 4-CP over Bi_2O_3/TiO_2 photocatalyst is feasible. The analyses of degradation intermediates by GC-MS and the ESR signals reveal the possible pathways during the 4-CP photodegradation.

Acknowledgements: We are grateful to key Lab for Special Functional Materials, Ministry of Education, Henan University for the XPS and TEM measurement.

References:

[1] Hoffmann M R, Martin S T, Choi W, et al. *Chem. Rev.*, **1995**, **95**:69-96

[2] Fujishima A, Rao T N, Tryk D A. *J. Photochem. Photobiol. C*: *Rev.*, **2000**,**1**:1-21

[3] ZHANG Xia(张霞), MENG Hao(孟皓), CAO Xiang-Hui(曹向会). *Chinese J. Inorg. Chem.*(*Wuji Huaxue Xuebao*), **2009**,**25**(11):1947-1952

[4] REN Ling(任凌), YANG Fa-Da(杨发达), ZHANG Yuan-Ming(张渊明), et al. *Chinese J. Inorg. Chem.*(*Wuji Huaxue Xuebao*), **2008**,**24**(4):541-546

[5] Kisch H, Sakthivel S, Janczarek M, et al. *J. Phys. Chem. C*, **2007**,**111**:11445-11449

[6] Paola A D, Palmisano L, Venezia A M, et al. *J. Phys. Chem. B*, **1999**,**103**:8236-8244

[7] Zhang H, Ouyang S, Li Z, et al. *J. Phys. Chem. Solids*, **2006**, **67**:2501-2505

[8] Liu H, Yang W, Ma Y, et al. *Appl. Catal. A*, **2006**,**299**:218-223

[9] Bessekhouad Y, Robert D, Weber J. *Catal. Today*, **2005**,**101**: 315-321

[10]Zhang L S, Wang W Z, Yang J, et al. *Appl. Catal. A*, **2006**, **308**:105-110

[11]Fox M A, Dulay M T. *Chem. Rev.*, **1993**,**93**:341-357

[12]Rengaraj S, Li X Z. *Chemosphere*, **2007**,**66**:930-938

[13]Wang J, Jing L Q, Xue L P, et al. *J. Hazard. Mater.*, **2008**,**160**: 208-212

[14]Bian Z F, Zhu J, Wang S H, et al. *J. Phys. Chem. C*, **2008**, **112**:6258-6262

[15]Marc P T, Verónica G M, Miguel A B, et al. *Appl. Catal. B*, **2004**,**47**:219-256

[16]YANG Juan(杨娟), DAI Jun(戴俊), MIAO Juan(缪娟), et al. *Acta Chim. Sinica*(*Huaxue Xuebao*), **2009**,**67**(17):1973-1980

[17]Dohnal V, Fenclova D. *J. Chem. Eng. Data*, **1995**,**40**:478-483

[18]Zhang Q H, Gao L, Guo J K. *Appl. Catal. B*, **2000**,**26**:207-216

[19]Zhang J, Li M J, Feng Z C, et al. *J. Phys. Chem. B*, **2006**,**110**: 927-935

[20]Schuhl Y, Baussart H, Delobel R, et al. *J. Chem. Soc. Faraday Trans.*, **1983**,**79**:2055-2061

[21]Lin Y H, Wang D J, Zhao Q D, et al. *J. Phys. Chem. B*, **2004**, **108**:3202-3206

[22]Dimitrov V, Dimitriev Y, Montenero A. *J. Non-Cryst. Solids*, **1994**,**180**:51-54

[23]Jing L Q, Fu H G, Wang B Q, et al. *Appl. Catal. B*, **2006**,**62**: 282-291

[24]Zhang M H, Shi L Y, Yuan S, et al. *J. Colloid Interf. Sci.*, **2009**,**330**:113-118

[25]Gujar T P, Shinde V R, Lokhande C D. *Mater. Res. Bull.*, **2006**,**41**:1558-1564

[26]Zhao J, Wu T, Wu K, et al. *Environ. Sci. Technol.*, **1998**,**32**: 2394-2400

[27]Xin J H, Zhang S M, Qi G D. *React. Kinet. Catal. Lett.*, **2005**, **86**:291-298

[28]Ao Y H, Xu J J, Fu D G, et al. *Sep. Purif. Technol.*, **2008**,**61**: 436-441